

### **CdSe Nanocrystals Enable New Methods for Color-Selective Semiconductor Laser Fabrication**

Hans-Jürgen Eisler and colleagues from the Massachusetts Institute of Technology and Los Alamos National Laboratory have developed an optically pumped nanocrystal distributed-feedback (DFB) laser that uses wet chemistry methods to produce nanocrystal titania waveguides. The researchers report in the June 17 issue of *Applied Physics Letters* that the emission wavelength of the nanocrystals is a function of their size. The wavelength of the nanocrystal-based DFB laser is chosen by varying nanocrystal size and by adjusting the refractive index of the waveguides through the volume fraction of nanocrystals.

The research team determined the amplified spontaneous-emission profiles of the nanocrystal titania waveguides and matched them to appropriately spaced direct-feedback gratings to provide feedback and demonstrate lasing. A solution of CdSe and CdSe(ZnS) core-shell nanocrystals, synthesized to be resilient to alcoholic solvents and arranged into a titania matrix at high volume fractions, was spin-coated onto silica substrates and annealed at 200°C to produce a clear, nanocrystal titania composite film. These samples were used to determine emission profiles. In the production of the lasers, the refractive index of the film was adjusted through its nanocrystal volume fraction to match the Bragg condition of lithographic gratings with periodicities of 310–350 nm. The gratings were fabricated by reactive ion etching on the 1- $\mu\text{m}$ -thick thermal oxide grown on silicon substrates, then the appropriate nanocrystal titania film was deposited. To test the resulting structures, the samples were initially cooled to 80 K, and a 400-nm pulsed excitation light was focused onto the structures. The resulting photoluminescence emission was coupled into a spectrometer and examined with a CCD camera. Emission from the front of the structure collapses into a visible laser beam, the researchers reported.

Alternatively, several direct-feedback lasers operating in the 560–625-nm range were created using a 350-nm grating periodicity, but the size and volume fraction of the constituent nanocrystals was varied, demonstrating the ability to tune the wavelength of these lasers, for a given grating periodicity, using only the nanocrystal size and volume fraction. These nanocrystal lasers exhibit thermal stability at room temperature and at 80 K.

The thermal stability and precise tunability of these nanocrystal lasers suggests that other materials may be suitable for the creation of nanocrystal lasers operat-

ing in the ultraviolet or infrared regimes.

CHRISTINE RUSSELL

### **Cobalt-Based Metal Oxide Negative Electrodes May Enable Practical Low-Voltage Li-Ion Cells**

The rapid development of innovative technologies in portable electronics for new and efficient power sources has led to great interest in lithium-ion batteries, due to their excellent electrochemical performance and design flexibility. With the continuing trend toward lower operating voltage in electronic devices, a lower-voltage Li-ion cell with large capacity and reversibility is desirable. To improve device performance,

researchers from Telcordia Technologies in Red Bank, N.J., and LRCS at the Université de Picardie Jules Verne in Amiens, France, were able to optimize the Li-ion cells using three-dimensional (3D) metal oxides, specifically CoO and Co<sub>3</sub>O<sub>4</sub>, as an alternative negative-electrode composite. Both cobalt-based metal oxides show comparable performance with the present-day Li-ion batteries at a lower operating voltage, with the combination of Li<sub>1+x</sub>Mn<sub>2</sub>O<sub>4</sub> positive electrode.

As reported in the June issue of *Electrochemical and Solid-State Letters*, F. Badway and co-workers first used the polyol process to prepare monodisperse

## **Cost-Effective Portable Spin Coater**



### **Two-Stage Spinning**

Dispense liquid during Stage 1  
Spin-up and flatten during Stage 2

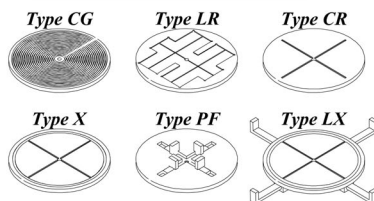
### **Adjustable Speed**

#### **Stage 1**

500 to 2500 rpm  
2 to 18 seconds

#### **Stage 2**

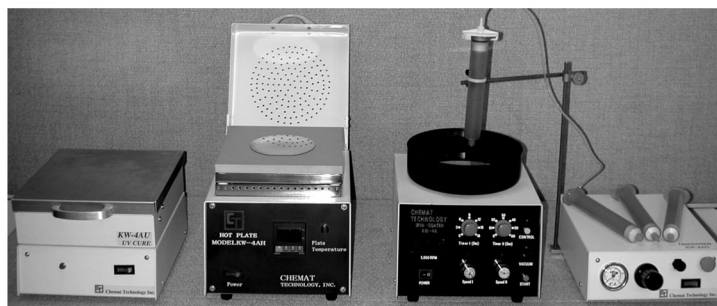
1,000 to 8,000 rpm  
3 to 60 seconds



### **Vacuum Chucks**

**Wide Range of Vacuum Chucks Available To Hold Different Substrates in KW-4A Spin Coater**

### **KW-4A SERIES PRODUCT LINE**



**UV Curer**  
KW-4AC

**Hot Plate**  
KW-4AH

**Spin Coater**  
KW-4A

**Dispenser**  
KW-4AD



### **CHEMAT TECHNOLOGY, INC.**

9036 Winnetka Avenue, Northridge, CA 91324  
1-800-475-3628, Fax: 818-727-9477

website: [www.enlabproducts.com](http://www.enlabproducts.com) ; [www.chemat.com](http://www.chemat.com)  
email: [marketing@chemat.com](mailto:marketing@chemat.com)

**Circle No. 4 on Inside Back Cover**

spherical particles of CoO and Co<sub>3</sub>O<sub>4</sub> that have specific surface areas smaller than 5 m<sup>2</sup>/g. Standard coin cells were assembled in a helium-filled glove box, which contains a plastic positive-electrode disk and a 1-cm<sup>2</sup> Li foil (as the negative-electrode member), thermally laminated to the metal grid current collectors. A borosilicate glass-fiber sheet, used as a separator, was saturated with a 1 M LiPF<sub>6</sub> electrolyte solution in a 1:1 (by weight) dimethyl carbonate/ethylene carbonate. Electrochemical tests were performed using an automatic cycling and data-recording system.

A series of different mass ratios ( $M_r$ ) of CoO/LiCoO<sub>2</sub> and Co<sub>3</sub>O<sub>4</sub>/LiCoO<sub>2</sub> were attempted to optimize electrochemical performance as a function of particle size. Results showed that the best electrochemical performance is achieved at a particle size of 1  $\mu$ m. Both systems were able to discharge and recharge for at least 80 cycles at a higher  $M_r$  with only minimal capacity decay at room temperature and 100% capacity retention for up to 50 cycles, after an initial irreversible capacity loss during the first cycle. At higher temperature, capacity loss for both Li-ion cells was not significantly affected.

To bypass the capacity loss during the first cycle, the researchers replaced the LiCoO<sub>2</sub> positive-electrode material with Li<sub>1+x</sub>Mn<sub>2</sub>O<sub>4</sub> as a Li reservoir. By applying this strategy, they were able to compensate the initial irreversible capacity loss. Further calculations also support the researchers' observations that the performance of the 3D metal oxide electrodes is comparable to commercialized C/LiCoO<sub>2</sub> Li-ion cells, at a lower voltage.

KINSON C. KAM

### 3D Tungsten/SiO<sub>2</sub> Structure Yields Infrared Photonic Bandgap

Three-dimensional (3D) arrangements of tungsten rods embedded in SiO<sub>2</sub> have been shown to have photonic bandgaps in the infrared region. S.Y. Lin and J.G. Fleming from Sandia National Laboratories and K.M. Ho and R. Biswas from the Ames Laboratory at Iowa State University have demonstrated this method for the fabrication of 3D tungsten crystals (W-3D) in the May 2 issue of *Nature*.

One of the challenges facing the development of metallic infrared-region photonics is the ability to selectively and precisely deposit or arrange arrays of metallic crystals in three dimensions. The researchers overcame this obstacle by utilizing micro-fabricated polysilicon/SiO<sub>2</sub> structures as crystal molds. The structure reported consisted of a polysilicon/SiO<sub>2</sub> photonic-bandgap structure with polysilicon rods in a stacking sequence inside the SiO<sub>2</sub> that

repeated itself every four layers, with a face-centered-tetragonal lattice symmetry. These polysilicon rods were removed by etching in 6 M KOH at 85°C. This effectively left linear voids in SiO<sub>2</sub>. An adhesion layer of TiN was then deposited, followed by chemical vapor deposition of tungsten, which resulted in W-3D crystals. Thin "keyholes" were located in the center of the tungsten rods. The tungsten layer was removed from the surface by mechanical polishing, and the SiO<sub>2</sub> was removed by HF (see Figure).

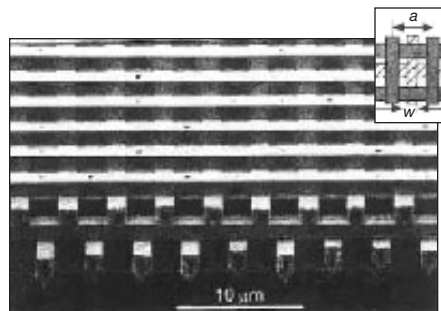


Figure. Scanning electron microscopy image of a three-dimensional tungsten crystal (W-3D); (inset) schematic illustration of the layered structure.

Optical measurements and computational estimates of the W-3D crystals were then carried out with reflectance and transmission Fourier transform infrared spectroscopy in the 1.5–25- $\mu$ m region. Reflectance measurements revealed oscillations at  $\lambda < 5.5 \mu$ m, with a sharp rise beginning at 6  $\mu$ m that peaked with a 90% reflectance when  $\lambda > 8 \mu$ m. Transmission measurements agreed with these values, with oscillation peaks close to  $\lambda < 5.5 \mu$ m, a sharp decrease at 6  $\mu$ m that revealed less than 1% transmission for  $\lambda > 8 \mu$ m. From this, the band edge was calculated to be  $\sim 6 \mu$ m. Large attenuation values of  $\sim 30$  dB at  $\lambda > 10 \mu$ m for a four-layer system were also observed. Comparisons of the optical properties of multilayer structures with those of a thin tungsten film demonstrate the effects of the photonic bandgap. Even though the photonic-bandgap structures are relatively opaque in the spectral region above 6  $\mu$ m, all have large values of transmission in the spectral region below 6  $\mu$ m, whereas the thin film is opaque across the entire spectral region characterized.

This data was also compared with transfer-matrix calculations. Here, the experimental and theoretical calculations were in agreement, with slight variations in transmission and reflectance maxima and peak widths. The researchers believe

one reason for the difference may come from the "keyholes" in each photonic tungsten rod. Because each rod is hollow to a small extent, scattering may have a significant impact. Furthermore, the bandgap attenuation was separated from typical metallic attenuation by the use of multilayer crystals (multiple layers of the four-layer unit). Peak amplitude and spectral position were demonstrated to be a function of W-3D thickness, not metallic depth. To further probe the metallic photonic bandgap, tilt-angle transmission measurements were performed. In photonic fashion, the strong reflectance at  $>10 \mu$ m was shown to be stable at angles ranging from 10° to -60°. Finite-difference time-domain calculations were also performed to better understand potential energy interactions at the W-3D surface.

The researchers believe that a wide reflectance window (8–20  $\mu$ m) may prove useful in many applications, including incandescent lamps and other thermal photovoltaic devices.

MATHEW M. MAYE

### Shape-Memory Polymer System Developed for Medical Applications

One of the challenges in the area of biomaterials is the medical application of materials that possess shape-memory properties induced thermally, including polymers, hydrogels, metallic alloys, and ceramics. For example, the nickel titanium alloy Nitinol has been used in orthodontic self-adjusting wires, flexible eyeglass frames, and pliant guidewires and tools for "bloodless" surgery. The preparation of the metal alloy, however, is a time-consuming procedure involving heat treatment at elevated temperatures. In addition, the maximum deformation of the alloys is limited, the materials are expensive, they are not biodegradable, and many are not mechanically biocompatible. Making advancements in minimally invasive surgical procedures, Andreas Lendlein from the Institute for Technical and Macromolecular Chemistry, Germany, and Robert Langer from the Department of Chemical and Biomedical Engineering at the Massachusetts Institute of Technology have introduced degradable thermoplastic polymers that can change their shape quickly at milder temperatures than other known shape-memory materials. Compared to known shape-memory alloys, these polymers are much more deformable and less expensive to produce.

As reported in the May 31 issue of *Science*, the linear phase-segregated multi-block copolymers were chosen as the